Registration and analysis of the shape fluctuations of nearly spherical lipid vesicles

Julia Genova,[*] Victoria Vitkova,[†] and Isak Bivas[‡]
Institute of Solid State Physics, Bulgarian Academy of Sciences, 72 Tzarigradsko Chaussee Boulevard, Sofia 1784, Bulgaria
(Received 10 June 2013; published 12 August 2013)

The analysis of shape fluctuations of giant nearly spherical lipid vesicles observed via optical microscopy is one of the widely used methods for the determination of the bending elasticity of lipid membranes. Although the method has been used already for three decades, the values of this material constant, obtained by different groups for membranes of the same composition, in identical conditions, differ significantly. The aim of the present work is the development of the method, enabling us to avoid the influence of artifacts on the value of the measured bending modulus. This is achieved by rejection of some images of the vesicle or the whole vesicle when they do not satisfy the requirements (selection criteria) of the applied theory. The bending modulus of 1-stearoyl-2-oleoyl-sn-glycerol-3-phosphocholine lipid membranes is determined via the advanced method described here. The results are compared with the values in the literature and their difference is discussed.

DOI: 10.1103/PhysRevE.88.022707 PACS number(s): 87.16.dj, 82.70.Uv, 87.16.dm, 82.70.Kj

I. INTRODUCTION

Giant unilamellar lipid vesicles, the simplest model of the complex biological cell, are the preferred objects for the study of important physical properties (mechanical, electrical, rheological, etc.) of biomembranes and the influence of various additives on these properties [1]. Their size (radius of the vesicle greater than several micrometers) allows direct observation via optical microscopy. Giant unilamellar lipid vesicles are readily and reproductively formed with controlled composition and in desired aqueous solutions [2–9]. Their lipid membranes permit us to successively approach the structure of real living membranes in physiologically relevant conditions by adding proteins, cholesterol, carbohydrates, salts, etc., to the membrane and/or surrounding medium.

The mechanical properties of biomembranes are one of the physical factors ensuring the proper functioning of living matter. This is the reason for the interest in the investigation of these properties and their dependence on diverse physicochemical parameters (temperature, composition of the membrane and aqueous solutions, etc.). The mechanical properties of lipid membranes in their liquid state are characterized by their bending elasticity, saddle-splay bending elasticity, stretching elasticity, and spontaneous curvature [10].

Various methods for the investigation of the mechanical properties of lipid membranes have been developed and used for the past few decades. Some of them are based on the response of the lipid membrane to the applied force: mechanical deformation by micropipette aspiration [11–13], electric field [14–18], optical force [19], etc. Others are based on the observation and analysis of the thermal shape fluctuations of tubular [20,21] or nearly spherical vesicles [18,21–28]. The latter class of experimental methods has the advantage of being noninvasive and applicable in a variety of aqueous solutions around the membrane, including a pure water environment. In recent years these experimental methods have been improved in terms of the experimental setup as well as the processing of the acquired data.

A typical experiment for analyzing the shape fluctuations of nearly spherical lipid vesicles consists in the acquisition of many images of the equatorial cross section of the fluctuating vesicle, taken at equal time intervals. The equatorial cross section of a fluctuating nearly spherical lipid vesicle is recorded using a CCD camera for a given period of time (approximately 5–10 min). The obtained sequence of images is analyzed and two mechanical characteristics of the vesicular membrane (bending elasticity modulus and membrane tension) are calculated. Due to diffusion processes in the water environment, the studied vesicle is chaotically moving within the experimental volume, thus generating a given amount of out-of-focus images and requiring periodic refocusing of the object of interest. Due to the finite integration time of the CCD camera, the fastest deformations of the membrane are smeared out, thus undesirably altering the calculated values of the mechanical constants. This blurring effect is overcome by using a short-impulse stroboscopic illumination [29] or a high-speed camera [18].

Various algorithms for detecting the points of the vesicle contour, representing the equatorial cross section of the vesicle, have been proposed for symmetrical and asymmetrical aqueous environments (with the same and different refractive indices of the solution inside and outside the vesicle, respectively) [25,28,30]. Later in this paper only symmetrical systems will be considered. Lipid vesicles are low-contrast objects, which is why they are observed via phase contrast microscopy. Under these conditions the algorithms used are based on extracting the minimum of the intensity profile in both horizontal and vertical directions [25], using a weighted mean in four directions of the profile [30], or fitting the intensity profile along a given direction with a Lorentzian function [28].

Lipid vesicles can be formally divided into two classes: vesicles without defects, which are appropriate for experimental treatment, and vesicles with defects (sometimes invisible like thin threads, connecting them to other vesicles or lipid packages) that have to be taken from the acquired set of data. An objective criterion for qualification of a given vesicle has to be introduced. An example for such a criterion, based on a

[*]ulia@issp.bas.bg
[†]victoria@issp.bas.bg
[‡]bivas@issp.bas.bg

comparison of the vesicle behavior with the model predictions, has been proposed by Méléard *et al*. [28].

In the case of high-quality vesicles, a set of good (mandatory focused) and bad (out-of-focus or with disconnected momentum defects in the focal plane of observation) images is recorded. A soft criterion for acceptance or rejection of a given image in the sequence has been proposed [31], taking into consideration the relative change in the length of the contour of the equatorial cross section of the studied vesicle or the area enclosed by it. Still there is much to be done in the way of having an automated vesicle digitization and processing algorithm that imposes strict objective criteria for selection of high-quality nearly spherical stationary vesicles and rejection of the bad contours in the image sequence of a given liposome. The large scattering of the values published in the literature so far for the bending elasticity modulus for a given type of lipid membranes [18,32,33] testifies to the necessity of establishing an artifact-free experimental procedure for the determination of this material constant. In this paper we propose an algorithm for digitalization and processing of image sequences of fluctuating vesicles with a detailed procedure for obtaining the mechanical constants of the vesicular membrane, applying strict objective criteria for qualification of the vesicle as a whole as well as for acceptance or rejection of a given contour of the sequence of recorded images.

II. MATERIALS

Giant vesicles were prepared from 1-stearoyl-2-oleoyl-sn-glycerol-3-phosphocholine (SOPC, Avanti Polar Lipids Inc., AL, USA) in water with pH $\sim$ 5.5 (double distilled in quartz distiller). Electroformation [2] was performed on indium-tin oxide (ITO) electrodes (100 $\pm$ 20 nm of ITO with a resistance of 20 Ω/Square) in specially constructed hermetic chambers [34]. As a result, dilute suspensions of fluctuating vesicles without observable defects on their membranes were produced and consequently used for membrane fluctuation analysis. The observation chamber consisted of an objective glass, a cover slip, and an inert spacer with a thickness of 0.5 mm (CoverWell, Sigma-Aldrich Inc., USA).

III. OBSERVATION AND REGISTRATION OF VESICLE IMAGES

Sample observation and registration were performed in phase contrast with an inverted Axiovert 100 (Zeiss, Germany) microscope equipped with an oil-immersed objective (100×, with a numerical aperture of 1.25). A CCD camera (C3582, Hamamatsu Photonics, Japan) was mounted on the microscope and connected to the video input of a frame grabber board (DT3155, Datatranslation, USA), installed in a computer for the digitization of the registered video signal in 768 × 576 eight-bit pixel format with a pixel size of 0.106 μm/pixel. In order to capture the fast modes of the vesicle fluctuations, which otherwise would be smeared due to the finite integration time (40 ms) of the camera, stroboscopic illumination of the sample was applied using a Xenon Flash Lamp (L6604, Hamamatsu, Japan) [29,35]. Images of the equatorial cross section of the fluctuating vesicle with the focal plane of the objective were acquired in real time (25 frames per second), digitized and recorded on a PC in order to obtain a long image sequence ($\sim 10^4$ frames).

For the deduction of the bending modulus at the free exchange of molecules between the two monolayers comprising the bilayer (free flip-flop [10]) every 25th frame is taken from the recorded image sequence [25–27]. Thus a new sequence for the given vesicle is obtained with a lapse of 1 s between two adjacent frames. In most cases the fluctuations of the contour recorded in these frames are not correlated. If necessary, the time lapse can be increased to ensure the independence of the fluctuations. The lack of correlation between the fluctuations permits us to use standard statistical methods for the calculation of the mean values and their errors of an ensemble of numbers.

IV. ACQUISITION AND ANALYSIS OF THE VESICULAR CONTOUR FLUCTUATIONS

When using phase-contrast microscopy, the lipid membrane of a vesicle is seen as a dark ring, clearly distinguishable on a bright background (see Fig. 1). The assumption is made that if for some image a profile of the intensity along the pixel rows or columns of the image, given in 255 levels of gray, is determined, the points (if they exist) belonging to the contour and lying on the corresponding row or column are those with a minimum of illumination. In our experimental equipment the width of the peaks around these minima are determined by the spatial resolution of the optical system and appear to be about 6–7 pixels. The existence of noises of various origin makes the minima not clearly defined and their positions cannot be determined with satisfactory accuracy. To overcome this problem, every image frame is divided into groups of 3 × 3 pixels and each group is replaced by one

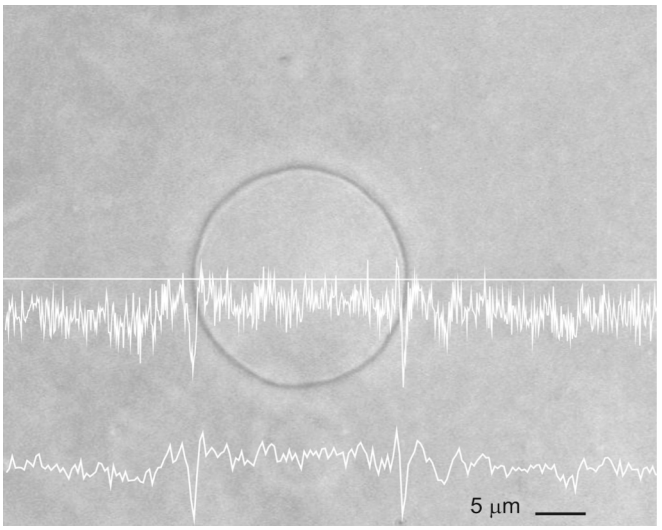

FIG. 1. Phase-contrast image of a vesicular contour. The upper white fluctuating line presents the profile of the light intensity along the straight white line before the coarse graining of the pixels, while the lower fluctuating line shows the scaled profile after the coarse graining (for details see the text). The cross points of the straight line with the contour are characterized by minima in the profile.

pixel with illumination equal to the average of those of the nine pixels. In this way, a new set of coarse-grained images is constructed, having three times greater pixel size. The noise in the coarse-grained images is considerably reduced due to the filtering of its higher frequencies. As a result, the accuracy of determining the position of the contour point on a given row (or column) is not worse than one-half of a pixel. It is worth noting that the coarse graining applied by us is not equivalent to a smoothing of the image. Later in this work, only the images obtained after the coarse graining of the pixels of the initial ones are considered.

Let a laboratory frame of reference $X'O'Y'$ be attached to the focal plane of the microscope. Let its axis X' be parallel to the rows of the image and the axis Y' be parallel to its columns. Let a frame of reference XOY be attached to an image of the fluctuating vesicle. Let its axes X and Y be parallel to X' and Y', respectively. Let the origin O coincide with the contour center, whose coordinates (x', y') in $X'O'Y'$ have been previously determined [25,26] and appropriately scaled after the coarse graining of the pixels of the original image.

Our procedure for extracting the contour from the image and the determination of its quality (good or bad) is the following. By means of homemade acquisition software, direct measurement of the vesicle radius R_{ves} in pixels on a randomly chosen image from the image sequence is made. Its approximate value is necessary for the further image processing. The determination of the contour continues by defining a region of interest (ROI) representing a ring containing the vesicular contour (see Fig. 2). The center of the ROI is made to coincide with the center of the contour. The ROI is delimited by two concentric circumferences with radii R_{int} and R_{ext} ($R_{\text{int}} < R_{\text{ves}} < R_{\text{ext}}$), between which the contour lies.

The scan of the intensity along the rows and columns is done only inside the ROI. As a result, two points of the contour along every row and two along every column inside the ROI are found, for which the profile intensity has its minimal

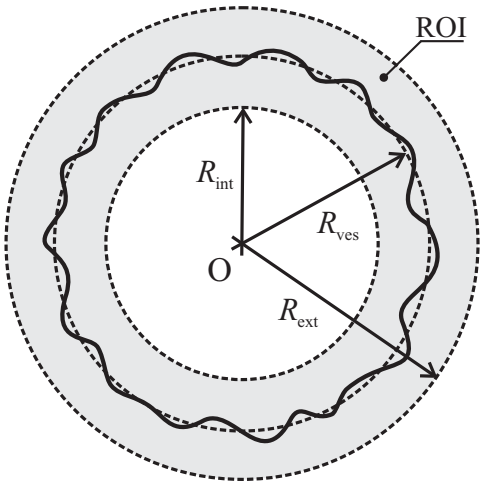

FIG. 2. Region of interest (ROI) representing a ring, containing the vesicular contour. The ROI is delimited by two concentric circumferences with radii R_{int} and $R_{\text{ext}}(R_{\text{int}} < R_{\text{ves}} < R_{\text{ext}})$, between which the contour lies. The center of the ROI coincides with the center of the contour. Here R_{ves} is the vesicle radius.

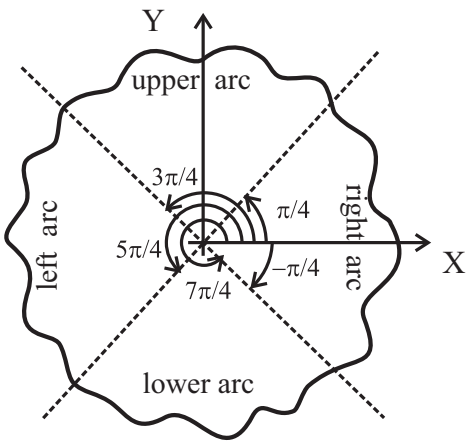

FIG. 3. Schematic representation of the equatorial cross section of a vesicle. Here O is the center of the vesicle, lying on the focal plane of the microscope, and XOY is a frame of reference with an origin O and axes X and Y, parallel to the rows and the columns of the image, respectively. The contour consists of four arcs: right, upper, left, and lower. The polar angles φ_{right}, φ_{upper}, φ_{left}, and φ_{lower} of the points, belonging to each of the four arcs, satisfy the inequalities $-\pi/2 < \varphi_{\text{right}} < \pi/2$, $\pi/2 < \varphi_{\text{upper}} < 3\pi/2$, $3\pi/2 < \varphi_{\text{left}} < 5\pi/2$, and $5\pi/2 < \varphi_{\text{lower}} < 7\pi/2$, respectively.

value (see Fig. 1). In this way, four rough arcs are obtained, the right and the left, from the minima of the profiles along the X' axis, and the upper and the lower, from the minima of the profiles along the Y' axis (see Fig. 3). Each right or left rough arc is interrupted at the point x having at least one neighbor from the two adjacent rows, whose coordinate differs from the x coordinate of the point with more than four pixels. The final (right or left) arc is enclosed between interruption points, nearest the axis X, above and below this axis. The final upper and lower arcs are determined in exactly the same manner.

In what follows, the criteria for the goodness of the contours, extracted from the image sequence, are presented and discussed. The contour is not rejected if the four arcs overlap so as to obtain a continuous contour and if this contour does not touch the circumferences of the ROI. In this way, out-of-focus frames or contours corrupted by the presence of optical defects in the background image are disregarded in the further analysis. This step represents the first criterion for rejection of a contour.

Further, the upper half of the right arc of the contour is considered (see Fig. 4). Let A and B be points of this part of the contour, belonging to two adjacent rows. Let these points have coordinates (x_A, y_A) and (x_B, y_B) and polar angles φ_A and φ_B in the frame XOY. The coordinates are measured in coarse-grained pixels. Let $y_B > y_A$ and $y_B - y_A = 1$. We denote by F_{AB} the expression, conjugated to the couple of points AB,

$$F_{AB} = x_A - x_B - \tan(\varphi_A). \tag{1}$$

As shown in Appendix A, in our experimental setup the probability for the modulus of F_{AB} to be greater than four pixels is negligible for a good contour. Consequently, a contour possessing one or more pairs of points of the kind described above with such a value of the corresponding expression can

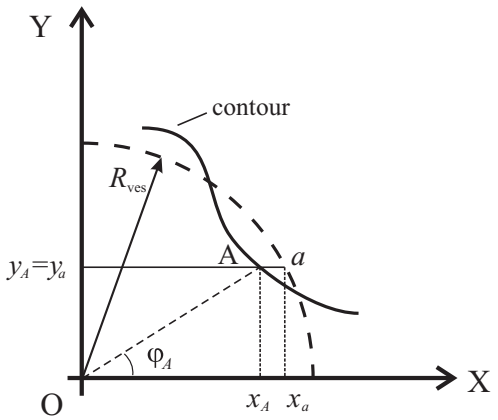

FIG. 4. Part of the contour representing the equatorial cross section of the vesicle. Here XOY is a frame of reference, similar to that of Fig. 3. A capital letter (say, A) denotes a point of the contour with coordinates (x_A, y_A). The corresponding lowercase letter (in this case, a) denotes the point with coordinates (x_a, y_a), lying on a circumference with center O and a radius, equal to the radius R_{ves} of the vesicle and having the property $y_A = y_a$.

be classified as bad and rejected from the sequence of accepted contours.

Exactly in the same manner we can determine the respective expression for two points, belonging to two adjacent rows from the lower half of the right arc or from the left arc of the contour. For the contour points of the upper and of the lower arcs, obtained via scanning of the light intensity along the columns, the y coordinates and the polar angles measured with respect to the axis Y have to be used.

The restrictions on the values of the quantity F_{AB} (and the corresponding quantities for each of the four arcs building up the contour) presented above is our second criterion for determining and eliminating bad contours. The coordinates of the center O of the contour in the $X'O'Y'$ are defined as the average of the x' and the y' coordinates of the contour points in this frame.

A number N of rays starting from the center and making angles $2\pi n/N$, $n = 1,2,\ldots,N$, with the axis X of the laboratory frame of reference are traced. The N rays determine N sectors with equal angles $2\pi/N$. The contour is not rejected if in each of these N sectors there is at least one of the contour points obtained above. This is the third criterion for rejection of a contour.

The sector between the nth and the $(n+1)$th ray is numbered with n, $n < N$, and the sector between the Nth and the first ray with N. Let r_n be the distance between the center O of the contour and the point of the contour with the lowest illumination among the points in the nth sector. An assumption is made that the length of the radius vector of the point where the nth ray intersects the contour is equal to r_n.

The contour of the equatorial cross section can be presented as an ensemble of radius vectors $\mathbf{R}(\varphi,t)$ in the frame of reference XOY, where φ are the polar angles of the contour points and t is the time of the registration (it can be determined knowing the number of the image and the time between two consecutive images: 40 ms in our setup). In this way each accepted contour is presented by a discrete ensemble of N points with radius vectors $\mathbf{R}(2\pi n/N,t)$, $n = 1,2,\ldots,N$.

The optimal values for the radii R_{int} and R_{ext} of the ROI are those for which the number of approved contours is maximal. Usually these are about 90% of all contours in the sequence. The outsourced data contain the numbers of the rejected images from the full record of the fluctuating vesicle and the distances between the center of the contour and each of its points in the N directions defined above for each of the approved images.

One of the possibilities to recover all the contour $R(\varphi,t)$ (evidently with some precision) is to present it in the form

$$R(\varphi,t) = R_{ves}\left\{1 + a_0 + \sum_{n=1}^{N/2-1}[a_n(t)\cos(n\varphi) + b_n(t)\sin(n\varphi)] + a_{N/2}(t)\cos\left(\frac{N}{2}\varphi\right)\right\}, \quad (2)$$

where R_{ves} is the radius of a sphere with volume equal to that of the vesicle. The Fourier amplitudes $a_n(t)$ and $b_n(t)$ can be determined from the known values of the radius vectors $R(2\pi n/N,t)$, $n = 1,2,\ldots,N$. The choice of $N = 2^k$ permits us to determine these amplitudes via a fast Fourier transform (FFT).

The assumption that $R(\varphi,t)$ can be presented in the form of Eq. (2) does not take into account the existence of harmonics with $n > N$. We are interested in amplitudes of harmonics with relatively low values, usually $n \leqslant 19$. The rejection of higher-order harmonics influences mainly the amplitudes around N. If the value of N is high enough, the influence on the amplitudes of the low-order harmonics is expected to be negligible.

The following step consists in the calculation of the autocorrelation function $\xi(N,\gamma)$ defined as [24]

$$\xi(N,\gamma) = \left\langle \frac{1}{2\pi}\int_0^{2\pi} \frac{[R(\varphi,t) - R_{ves}][R(\varphi+\gamma,t) - R_{ves}]}{(R_{ves})^2} d\varphi \right\rangle, \quad (3)$$

where $\langle A(t)\rangle$ denotes the time average of the time-dependent quantity $A(t)$ and $\xi(N,\gamma)$ is calculated from the amplitudes $a_n(t)$ and $b_n(t)$ [see Eq. (2)], obtained from the experimental data via a FFT. The function $R(\varphi,t)$ can be presented as

$$R(\varphi,t) = R_{ves} + \Delta R^{fluct}(\varphi,t) + \Delta R^{noise}(\varphi,t), \quad (4)$$

where $\Delta R^{fluct}(\varphi,t)$ are the changes of the radii due to the thermal shape fluctuations of the vesicle and $\Delta R^{noise}(\varphi,t)$ are the alterations of the radii due to the experimental errors in the determination of the quantities $R(2\pi n/N,t)$, $n = 1,2,\ldots,N$. These errors are considered as white noise, i.e., they are normally distributed around zero with respect to time; the errors for different values of n are not correlated and their variances do not depend on n. Because of their different origins, $\Delta R^{fluct}(\varphi,t)$ and $\Delta R^{noise}(\varphi,t)$ are not time correlated:

$$\langle \Delta R^{fluct}(\varphi,t) \times \Delta R^{noise}(\varphi+\gamma,t)\rangle = 0. \quad (5)$$

As a result, $\xi(N,\gamma)$ can be presented as

$$\xi(N,\gamma) = \xi^{fluct}(N,\gamma) + \xi^{noise}(N,\gamma), \quad (6)$$

where $\xi^{\mathrm{fluct}}(N,\gamma)$ is determined by $\Delta R^{\mathrm{fluct}}(\varphi,t)$ and $\xi^{\mathrm{noise}}(N,\gamma)$ by $\Delta R^{\mathrm{noise}}(\varphi,t)$:

$$\xi^{\mathrm{fluct}}(N,\gamma) = \left\langle \frac{1}{2\pi}\int_0^{2\pi} \frac{[\Delta R^{\mathrm{fluct}}(\varphi,t)][\Delta R^{\mathrm{fluct}}(\varphi+\gamma,t)]}{(R_{\mathrm{ves}})^2} d\varphi \right\rangle \quad (7)$$

and

$$\xi^{\mathrm{noise}}(N,\gamma) = \left\langle \frac{1}{2\pi}\int_0^{2\pi} \frac{[\Delta R^{\mathrm{noise}}(\varphi,t)][\Delta R^{\mathrm{noise}}(\varphi+\gamma,t)]}{(R_{\mathrm{ves}})^2} d\varphi \right\rangle. \quad (8)$$

The function $\xi(N,\gamma)$ can be decomposed into a series with respect to the Legendre polynomials $P_l[\cos(\gamma)]$ [25] as

$$\xi(N,\gamma) = \sum_{l=0}^{N-1} B_l(N) P_l[\cos(\gamma)], \quad (9)$$

where N is the number of rays starting from the center of the contour. The amplitudes $B_l(N)$ can be presented as

$$B_l(N) = B_l^{\mathrm{fluct}}(N) + B_l^{\mathrm{noise}}(N), \quad (10)$$

where

$$\xi^{\mathrm{fluct}}(N,\gamma) = \sum_{l=0}^{N-1} B_l^{\mathrm{fluct}}(N) P_l[\cos(\gamma)] \quad (11)$$

and

$$\xi^{\mathrm{noise}}(N,\gamma) = \sum_{l=0}^{N-1} B_l^{\mathrm{noise}}(N) P_l[\cos(\gamma)]. \quad (12)$$

As shown elsewhere [25], for $l \geqslant 2$, $B_l^{\mathrm{fluct}}(N)$ are given by the expression

$$B_l^{\mathrm{fluct}}(N) = \frac{kT}{4\pi k_c} \frac{2l+1}{(l-1)(l+2)[l(l+1)+\overline{\sigma}]}, \quad (13)$$

where kT is the Boltzmann factor, k_c is the bending elasticity modulus of the vesicle membrane [10], and $\overline{\sigma} = \sigma(R_{\mathrm{ves}})^2/k_c$ is the normalized membrane tension, where σ is the real tension of the membrane.

To calculate $\xi^{\mathrm{noise}}(N,\gamma)$ we introduce the quantities $h_n(N,t)$, $n = 1,2,\ldots,N$ as follows:

$$h_n(N,t) = \frac{\Delta R^{\mathrm{noise}}(2\pi n/N,t)}{R_{\mathrm{ves}}}. \quad (14)$$

As $h_n(N,t)$ are relevant to white noise [see the text after Eq. (4)], the time mean squares $\langle [h_n(N,t)]^2 \rangle$ do not depend on n under the assumption that no systematic errors originating from the microscope or other sources exist. We denote their values by

$$\overline{[h(N)]^2} = \langle [h_n(N,t)]^2 \rangle. \quad (15)$$

The quantity $h(N)$ has the meaning of a standard deviation of the white noise, presented by the functions $h_n(N,t)$. Assuming $\Delta R^{\mathrm{noise}}(2\pi n/N,t) \sim 0.5$ pixel and $R_{\mathrm{ves}} \sim 35$ pixel (typical for our experiments), we estimate $\overline{[h(N)]^2} \sim 0.25 \times 10^{-3}$.

As shown in Appendix B, $\xi^{\mathrm{noise}}(N,\gamma)$ can be expressed by $\overline{[h(N)]^2}$ in the following way:

$$\xi^{\mathrm{noise}}(N,\gamma) = \frac{\overline{[h(N)]^2}}{N}\left[1 + 2\sum_{n=1}^{N/2-1}\cos(n\gamma) + \frac{1}{2}\cos\left(\frac{N}{2}\gamma\right)\right]. \quad (16)$$

Again, there it is shown that $\xi^{\mathrm{noise}}(N,\gamma)$ can be decomposed into a series with respect to the Legendre polynomials $P_l[\cos(\gamma)]$ with amplitudes $B_l^{\mathrm{noise}}(N)$ [see Eq. (12)]:

$$B_l^{\mathrm{noise}}(N,\gamma) = (2l+1)\frac{2\overline{[h(N)]^2}}{N^2} F(N,l). \quad (17)$$

Since the quantity $\xi^{\mathrm{noise}}(N,\gamma)$ is an interpolation of the correlations $\langle R(2\pi n'/N,t) R(2\pi n''/N,t)\rangle \sim \delta_{n'n''}$ ($\delta_{n'n''}$ is the Dirac symbol and $n',n'' = 1,2,\ldots,N$) of the radius fluctuations $R(2\pi n/N,t)$, it must be independent of N at $\gamma = 0$. The quantity $\xi^{\mathrm{noise}}(N,\gamma)$ obtained above satisfies this requirement and is proportional to $1/N$. However, $\xi^{\mathrm{noise}}(N,\gamma)$ is a δ-like function of γ with width proportional to the distance between two adjacent pixels representing the contour, i.e., to $1/N$. Hence the amplitudes $B_l^{\mathrm{fluct}}(N,\gamma)$ must depend on $1/N^2$ as calculated here. The $F(N,l)$ in Eq. (17) are factors of the order of unity that were calculated numerically here and are given in Table I.

Finally, for $l \geqslant 2$,

$$B_l(N) = \frac{kT}{4\pi k_c}\frac{2l+1}{(l-1)(l+2)[l(l+1)+\overline{\sigma}]} + (2l+1)\frac{2\overline{[h(N)]^2}}{N^2} F(N,l). \quad (18)$$

This equation shows that there are three parameters k_c, $\overline{\sigma}$, and $\overline{[h(N)]^2}$ that must be calculated to fit the best dependence of B_l on them. So far, only the first two were taken into account

TABLE I. Numerically calculated values of the factors $F(N,l)$ from Eq. (17) for $N = 64$, 128, and 256 and $l = 2$–19.

	N		
l	256	128	64
2	1.004152892	1.008810030	1.019715027
3	1.000366401	1.001467890	1.005908441
4	1.004585808	1.010569908	1.027053663
5	1.000916758	1.003681894	1.014970679
6	1.005267238	1.013354144	1.038913577
7	1.001713325	1.006905978	1.028503621
8	1.006198701	1.017188205	1.055770420
9	1.002757865	1.011169340	1.047045044
10	1.007382278	1.022107776	1.078352039
11	1.004052701	1.016511367	1.071394929
12	1.008820635	1.028159702	1.107734640
13	1.005600731	1.022982664	1.102722266
14	1.010517029	1.035403275	1.145506234
15	1.007405448	1.030646445	1.142745978
16	1.012475336	1.043911924	1.194052940
17	1.009470958	1.039580339	1.194052940
18	1.014700072	1.053775412	1.257087409
19	1.011802008	1.049878725	1.260689379

in the fitting procedure [25]. As will be seen in Sec. V, in many cases the effects of the third parameter, appearing due to the white noise, have to be taken into account.

In the present study the calculation of $B_l(N)$ is carried out as follows. For the accepted contours, auxiliary autocorrelation functions $\xi^{\rm aux}(N,\gamma,t_i)$ are introduced, defined as

$$\xi^{\rm aux}(N,\gamma,t_i) = \frac{1}{2\pi}\int_0^{2\pi} \frac{[R(\varphi,t_i)-R_{\rm ves}][R(\varphi+\gamma,t_i)-R_{\rm ves}]}{(R_{\rm ves})^2}d\varphi, \tag{19}$$

where t_i is the moment of acquisition of the ith image. The N radius vectors $R(2\pi l/N,t_i)$, $l=1,2,\ldots N$, of the contour are determined and the Fourier amplitudes from Eq. (2) are calculated via a FFT. By means of these amplitudes the functions $R(\varphi,t_i)$ and $\xi^{\rm aux}(N,\gamma,t_i)$ are calculated.

Let $B_l^{\rm aux}(N,t_i)$ be the amplitudes of the decomposition of $\xi^{\rm aux}(N,\gamma,t_i)$ into a series with respect to the Legendre polynomials $P_l[\cos(\gamma)]$:

$$\xi^{\rm aux}(N,\gamma,t_i) = \sum_{l=0}^{N-1} B_l^{\rm aux}(N,t_i)P_l[\cos(\gamma)]. \tag{20}$$

Let M be the number of accepted contours. Then $B_l(N)$ is expressed by $B_l^{\rm aux}(N,t_i)$ as

$$B_l(N) = \frac{1}{M}\sum_{i'} B_l^{\rm aux}(t_{i'}), \tag{21}$$

where i' is the ensemble of numbers of accepted contours.

The fitting procedure for obtaining k_c, $\overline{\sigma}$, and $\overline{[h(N)]^2}$ and their errors from $B_l(N)$ requires the knowledge of the errors $\Delta B_l(N)$ of $B_l(N)$. If the time interval $\Delta t = t_i - t_{i-1}$ is long enough (1 s for the case when every 25th frame is taken from the recorded image sequence), the values of the amplitudes $B_l^{\rm aux}(t_{i'})$ are not correlated and then the standard procedure for the error determination can be applied:

$$\Delta B_l(N) = \sqrt{\frac{\sum_{i'}\left\{\left[B_l^{\rm aux}(N,t_{i'})\right]^2 - [B_l(N)]^2\right\}}{M-1}}. \tag{22}$$

A sufficient condition ensuring that $B_l^{\rm aux}(N,t_{i'})$ are not correlated is the validity of the inequality $\Delta t \gg \tau_2$, where τ_2 is the correlation time of the (slowest) modes with numbers $l=2$ in the decomposition of the vesicle shape fluctuations in a series with respect to the spherical harmonics $Y_l^m(\theta,\phi)$ [see Eqs. (A2) and (A3) in Appendix A] [36]. Here it is assumed that the inequality is fulfilled if $\Delta t > 2\tau_2$.

After the calculation of the mean values $B_l(N)$ and their standard deviations ΔB_l, the fitting parameters k_c, $\overline{\sigma}$, and $\overline{[h(N)]^2}$ are determined, ensuring the best fit of $B_l(N)$ with the theoretical results from Eq. (18). If the calculated goodness of fit is lower than 0.1, this is considered as an indication for hidden defects and the vesicle is rejected. This is the first of our criteria for the goodness of the treated vesicle.

The second criterion is the conservation of its volume during the experiment. The fulfillment of this requirement is controlled via the time evolution of the amplitudes of the second harmonics of the radius fluctuations. If such evolution exists, the vesicle volume and/or area is not conserved and the vesicle is rejected.

V. RESULTS AND DISCUSSION

In this section the experimental results for the bending elasticity of SOPC lipid bilayers are presented. They are obtained from the analysis of the shape fluctuations of nearly spherical lipid vesicles as described above.

As noted in Sec. III, the image sequences we processed consist of vesicle images registered every second during a period of ~7 min (i.e., about 400 images per vesicle). For vesicles with radii $R_{\rm ves} \sim 10\ \mu$m and with this frequency of registration the contour frames of the sequence are not correlated unless $\tau_2 \geqslant 0.5$ s [τ_2 depends on $R_{\rm ves}$ and $\overline{\sigma}$; see the text after Eq. (22)]. The inequality $\tau_2 \leqslant 0.5$ s was fulfilled for all the vesicles we considered. Thus the mean values and their standard deviations for the quantities related to the fluctuations were calculated using the standard methods for calculation applicable for ensembles of uncorrelated numbers with Gaussian distributions.

The ensemble of accepted vesicles included only samples satisfying all criteria for good vesicles. For each of them the bending elasticity modulus and its error were calculated. The fit of these bending elasticities with a constant k_c gave the following results for its value and its error (in ergs):

$$k_c = (1.88 \pm 0.17)\times 10^{-12}. \tag{23}$$

The fit of the experimental data presented above has a goodness of fit equal to 0.59. Consequently, the assumption that the membrane bending elasticity of the ensemble of vesicles is the same for all of them is relevant from a statistical point of view. This membrane property for different vesicles, which is obvious from a theoretical point of view, is experimentally shown to be in accord with statistical predictions, obtained from the experimental data.

For comparison, the value of the bending constant was estimated without accounting for the white-noise contribution. In order to quantify its effect on the calculated bending modulus, the experimental data were fitted without taking into account the terms corresponding to the white noise, i.e., the $\Delta R^{\rm noise}(\varphi,t)$ terms in the above equations were taken to be equal to zero. The value obtained, $k_c = (1.45 \pm 0.08)\times 10^{-12}$ ergs, is significantly lower than the value reported above [see Eq. (23)]. This result is consistent with previous experimental values for k_c of phosphatidylcholine bilayers found in the literature [18,32], where the white-noise contribution to the measured value of the bending modulus was not considered. Another important step in our analysis was to probe for any radius dependence of the calculated bending constant for every SOPC vesicle satisfying the criteria discussed in the preceding sections. From our experimental data no statistically significant dependence on $R_{\rm ves}$ is captured for either case, with and without accounting for the white-noise terms during the k_c calculation.

To ensure that the contours from an image sequence will not be rejected because of the third criterion for contour selection (see Sec. IV) it was shown that 64 directions presenting the fluctuating contour of the equatorial cross section of the vesicle must be taken for vesicles with radii less than 132 pixels. For this number of directions the effects of the quantity $\overline{[h(N)]^2}$ [see Eq. (15) and the text after it] are not negligible and it must

be taken into account in the fitting procedure, permitting the determination of k_c from the experimental data [see Eq. (18)].

The value of the bending modulus reported here is higher than those that can be found in the literature (see [18,32] and references therein). This difference is most probably due to two important reasons. The first one consists in the fact that in the present study the bad vesicles and the bad contours from the good vesicles, both of which artificially decrease this value, are rejected. The second important point is the accounting for the white-noise contribution in the thermal fluctuation analysis.

The values of the parameters of the experimental setup (magnification of the optical system, number of pixels per unit length, etc.) are essentially used in most of the estimations reported here. Obviously, for a different setup the estimations must be recalculated using the respective values.

ACKNOWLEDGMENTS

Financial support from the Science fund of the Bulgarian Ministry of Education and Science via Grant No. NTS01-121 is gratefully acknowledged. V.V. acknowledges also financial support via Grant No. DMU03-80/2011 from the National Science Fund (Bulgaria).

APPENDIX A: ESTIMATION OF THE DIFFERENCE OF THE COORDINATES OF TWO POINTS OF THE CONTOUR BELONGING TO TWO ADJACENT ROWS OR COLUMNS

A contour is considered, representing the cutoff of the vesicle, with the focal plane of the microscope (see Fig. 4). The vesicle is focused, i.e., the center of the vesicle lies on the focal plane. The contour is extracted from the image with coarse-grained pixels. For the conditions of our experimental setup, described in Sec. IV, the dimension of the pixel is $\sim 0.3\ \mu$m. Usually the radii $R_{\rm ves}$ (defined in Sec. IV) of the vesicles we studied were $\sim 10\ \mu$m, which corresponds to ~ 35 pixels. Later in the numerical estimations $R_{\rm ves} = 35$ is taken.

Let us consider first the upper half of the right arc of the contour. In the frame of reference XOY, introduced in Sec. IV, the points of this part have polar angles φ in the interval $(0,\pi/4)$ and are obtained from the scan of the light intensity along the rows of the image. Because of the symmetry, all the results obtained for this part of the contour will be valid for the other parts too.

We assume first that we dispose of the true contour representing a continuous two-dimensional planar curve. Its points are denoted by capital letters possessing an upper index 0.

Let A^0 be a point of the true contour with coordinates (x_{A^0}, y_{A^0}). Let φ_{A^0} be the polar angle of A^0. Then

$$\tan(\varphi_{A^0}) = \frac{y_{A^0}}{x_{A^0}}. \tag{A1}$$

Let a circumference with radius $R_{\rm ves}$ and center coinciding with the center of the vesicle be traced (see Fig. 4). A small letter, conjugated to the capital one and possessing an upper index 0 (in the considered case a^0), denotes the point lying on the circumference having coordinates (x_{a^0}, y_{a^0}) and possessing the property $y_{a^0} = y_{A^0}$. Let the oriented length $L_X^{A^0}$ of the segment A^0a^0, conjugated to the point A^0, be defined as $L_X^{A^0} = x_{A^0} - x_{a^0}$. This length can be determined for each of the points of the contour.

We proceed with the calculation of the oriented length $L_X^{A^0}$. Let $\boldsymbol{R}(\theta,\phi,t)$ be the radius vector of a point on the surface of the fluctuating vesicle at time t with polar angles (θ,ϕ) in a frame of reference with origin coinciding with the center of the vesicle and axis Z perpendicular to the focal plane of the microscope. The modulus $R(\theta,\phi,t)$ of this radius vector can be presented in the following way [36,37]:

$$R(\theta,\phi,t) = R_{\rm ves}[1 + u(\theta,\phi,t)], \tag{A2}$$

where $u(\theta,\phi,t)$ can be developed in a series with respect to the spherical harmonics $Y_l^m(\theta,\phi)$ as

$$u(\theta,\phi,t) = \sum_{l=2}^{l_{\max}} \sum_{m=-l}^{l} u_l^m(t) Y_l^m(\theta,\phi). \tag{A3}$$

In this equation $l_{\max}$ is of the order of the square root of the number of molecules in the vesicle membrane. The time mean squares of the amplitudes $u_l^m(t)$ satisfy the well known relation [36]

$$\left\langle \left| u_l^m(t) \right|^2 \right\rangle = \frac{kT}{k_c} \frac{1}{(l-1)(l+2)[l(l+1)+\overline{\sigma}]}, \tag{A4}$$

where kT, k_c, and $\overline{\sigma}$ are defined after Eq. (13).

Using the fact that the equatorial cross section of the vesicle corresponds to $\theta = \pi/2$ and that on this plane ϕ_{A^0} is equal to φ_{A^0}, the oriented length $L_X^{A^0}$ of the point A^0 (see Sec. IV and Fig. 4) is expressed to first-order precision with respect to $u_l^m(t)$ as

$$L_X^{A^0} \approx \frac{R_{\rm ves}}{\cos(\varphi_{A^0})} \left[\sum_{l=2}^{l_{\max}} \sum_{m=-l}^{l} u_l^m(t) Y_l^m\left(\frac{\pi}{2}, \varphi_{A^0}\right) \right]. \tag{A5}$$

Let B^0 be a point of the contour with coordinates (x_{B^0}, y_{B^0}) satisfying the condition $y_{B^0} = y_{A^0} + 1$ (in this way we take into account that B^0 lies on a row adjacent to that of the point A^0) and having polar coordinate φ_{B^0}. We define $\delta_{A^0B^0} = \varphi_{B^0} - \varphi_{A^0}$. It can be shown that with precision to first order with respect to u_l^m and $1/R_{\rm ves}$ this angle can be expressed as (the distances are measured in pixels)

$$\delta_{A^0B^0} \approx \frac{1}{R_{\rm ves}\cos(\varphi_{A^0})}. \tag{A6}$$

Let $L_X^{B^0}$ be the oriented length conjugated to B^0. Then the difference $x_{A^0} - x_{B^0}$ satisfies the relation

$$x_{A^0} - x_{B^0} - \tan(\varphi_{A^0}) = L_X^{A^0} - L_X^{B^0}. \tag{A7}$$

To estimate the order of magnitude of the fluctuations of $L_X^{A^0} - L_X^{B^0}$ due to the thermal fluctuations of the vesicle, we first find the time mean square $\langle (L_X^{A^0} - L_X^{B^0})^2 \rangle$. The result is

$$\begin{aligned} &\left\langle \left(L_X^{A^0} - L_X^{B^0}\right)^2 \right\rangle \\ &= (R_{\rm ves})^2 \frac{kT}{4\pi k_c} \sum_{l=2}^{l_{\max}} \left\{ \frac{2l+1}{(l-1)(l+2)[l(l+1)+\overline{\sigma}]} \right. \\ &\quad \times \left[\frac{1}{[\cos(\varphi_{A^0})]^2} + \frac{1}{[\cos(\varphi_{A^0} + \delta_{A^0B^0})]^2} \right. \\ &\quad \left. \left. - \frac{2P_l[\cos(\delta_{A^0B^0})]}{[\cos(\varphi_{A^0})][\cos(\varphi_{A^0} + \delta_{A^0B^0})]} \right] \right\}. \end{aligned} \tag{A8}$$

The quantities kT, k_c, and $\overline{\sigma}$ in this equation are defined after Eq. (13). The time mean square calculated above is an increasing function of φ_{A^0} in the interval $(0,\pi/4)$ and practically does not depend on R_{ves}. Taking $\frac{kT}{k_c} = \frac{1}{20}$, we find the value of this function to be 0.035 pixel^2 for $\varphi_{A^0} = 0$ and 0.14 pixel^2 for $\varphi_{A^0} = \pi/4$. Later on we assume that the distribution of $L_X^{A^0} - L_X^{B^0}$ due to the thermal fluctuations of the vesicle has properties not essentially different from those of a normal distribution around zero with an effective variance of 0.14 pixel^2 [slightly overestimated because the highest calculated value of $\langle (L_X^{A^0} - L_X^{B^0})^2 \rangle$ is taken].

Let us consider now the case when A and B are points of the contour, extracted from a coarse-grained image and consisting of discrete points. Let (x_A, y_A),(x_B, y_B) and φ_A,φ_B be their coordinates and polar angles, respectively. They can be presented as

$$\begin{aligned} x_A &= x_A^0 + \Delta x_A, \\ x_B &= x_B^0 + \Delta x_B, \\ \varphi_A &= \varphi_A^0 + \Delta\varphi_A, \\ \varphi_B &= \varphi_B^0 + \Delta\varphi_B, \end{aligned} \tag{A9}$$

where x_A^0, x_B^0, φ_A^0, and φ_B^0 are the true values of x_A, x_B, φ_A, and φ_B and Δx_A, Δx_B, $\Delta\varphi_A$, and $\Delta\varphi_B$ are their errors due to the finite size of the pixels. The fluctuations of the values of $F_{AB} = x_A - x_B - \tan(\varphi_A)$ are due also to the experimental errors of x_B, x_A, and $\tan(\varphi_A)$ determined from the experimental data [see Eq. (A7)].

As noted in Sec. IV, the precision of the determination of x_A and x_B is ~0.5 pixel. We assume that the distributions of these two errors are also normal. Their variances are equal to the square of their experimental error (appearing as a standard deviation of this distribution), i.e., 0.25 pixel^2 for each of them. Assuming that the error of y_A is also of the order of 0.5 pixel and taking into account that in the upper part of the right arc of the contour the coordinate x_A is between 17 and 35 pixels, we calculated a very low value for the error $\Delta\tan(\varphi_A)$ of $\tan(\varphi_A)$ and neglected it.

In summary, there are three essential contributions to the fluctuations of F_{AB}: the vesicle thermal shape fluctuations and the experimental errors in the measurements of x_A and of x_B. They are not correlated and are assumed with a normal distribution. In this case F_{AB} should have also a normal distribution around zero with variance Σ^2 equal to the sum of the three variances: $\Sigma^2 = 0.14$ pixel^2 + 0.25 pixel^2 + 0.25 pixel^2 = 0.64 pixel^2. The standard deviation Σ of F_{AB} is equal to the square root of its variance: $\Sigma = \sqrt{0.64 \text{ pixel}^2} = 0.8$ pixel.

One quantity with a normal distribution can take values in the whole interval $(-\infty,\infty)$. If restrictions on the values of F_{AB} are imposed, some part of the good contours will be rejected. We chose an interval of acceptable values of F_{AB}, ensuring that less than 1% of the good contours will be rejected. Taking into account that each contour contains ~200 points, it can be shown that the ensemble of good contours containing at least one pair of points A and B with F_{AB} satisfying the inequality $|F_{AB}| > 4\Sigma$ is about 1% of the whole ensemble of good contours; however, $4\Sigma = 3.2$ pixels. If a contour contains at least one pair of points A and B with $|F_{AB}| > 4$ pixels (taking into account that F_{AB} is a whole number, we choose the smallest whole number superior to our estimation), either it is bad or it is good with negligible probability. In both cases such a contour can be rejected.

APPENDIX B: INFLUENCE OF THE WHITE NOISE ON THE CALCULATION OF THE BENDING ELASTICITY

We consider the function $R(\varphi,t)$ from Eq. (2), which is periodic with respect to φ with period 2π. We define the function $h(\varphi,t)$ as $h(\varphi,t) = [R(\varphi,t) - R_{\text{ves}}]/R_{\text{ves}}$ [R_{ves} is defined after Eq. (2)]. Let N be a natural number with the property $N = 2^l$ [see the text after Eq. (2)]. We use the quantities, introduced in Eq. (14), $h_n(N,t)$, $n = 1,2,\ldots,N$. We assume that $h(\varphi,t)$ can be developed in a Fourier series containing N different amplitudes, as it was assumed for $R(\varphi,t)$ [see Eq. (2)]:

$$h(\varphi,t) = \frac{1}{N}\left\{ H_0(t) + \sum_{n=1}^{N/2-1} [H_n(t)\exp(in\varphi) + H_n^*(t) \times \exp(-in\varphi)] + H_{N/2}(t)\cos\left(\frac{N}{2}\varphi\right)\right\}, \tag{B1}$$

where i is the imaginary unit and $H_n^*(t)$ is complex conjugate to $H_n(t)$. In this equation $H_0(t)$ and $H_{N/2}(t)$ are real numbers and $h(\varphi,t)$ is a real function. Equation (B1) can be obtained from Eq. (2) after appropriate substitutions.

As noted after Eq. (14), we assume that the quantities $h_n(N,t)$ have the character of white noise not depending on n standard deviation. Consequently,

$$\langle h_k(N,t) h_l(N,t)\rangle = \delta_{kl}\overline{[h(N)]^2}, \tag{B2}$$

where δ_{kl} is the Dirac symbol and $\overline{[h(N)]^2}$ is defined via Eq. (15). From Eqs. (B1) and (B2) and from the relation

$$\sum_{k=0}^{N-1}\exp\left(i\frac{2\pi}{N}nk\right) = \delta_{n0}N \tag{B3}$$

we obtain

$$H_n(t) = \sum_{k=0}^{N-1} h_k(t)\exp\left(-i\frac{2\pi}{N}nk\right) \tag{B4}$$

and

$$\langle H_m(t) H_n^*(t)\rangle = \delta_{mn}N\overline{[h(N)]^2}. \tag{B5}$$

These results permit us to calculate the correlation $\langle h(\varphi,t)h^*(\varphi+\gamma,t)\rangle$:

$$\langle h(\varphi,t)h^*(\varphi+\gamma,t)\rangle = \frac{\overline{[h(N)]^2}}{N}\left\{1 + 2\sum_{n=1}^{N/2-1}\cos(n\gamma) + \frac{1}{2}\left[\cos\left(N\varphi + \frac{N}{2}\gamma\right) + \cos\left(\frac{N}{2}\gamma\right)\right]\right\}. \tag{B6}$$

After averaging this equation with respect to φ, Eq. (16) is obtained.

From Eqs. (12) and (16) we calculate the amplitudes B_l^{fluct} and obtain the result from Eq. (17). The numerical results for the factors $F(N,l)$ are presented in Table I.

[1] *Giant Vesicles*, edited by P.-L. Luisi and P. Walde (Wiley, Chichester, 2000).
[2] M. I. Angelova and D. Dimitrov, Faraday Discuss. Chem. Soc. **81**, 303 (1986).
[3] K. Akashi, H. Miyata, H. Itoh, and K. Kinosita, Jr., Biophys. J. **71**, 3242 (1996) .
[4] A. Moscho, O. Orward, D. Chiu, B. P. Modi, and R. Zare, Proc. Natl. Acad. Sci. U.S.A. **93**, 11443 (1996).
[5] D. J. Estes and M. Mayer, Biochim. Biophys. Acta **1712**, 152 (2005).
[6] M. M. Lapinski, A. Castro-Forero, A. J. Greiner, R. Y. Ofoli, and G. J. Blauchard, Langmuir **23**, 11677 (2007).
[7] R. L. Montes, A. Alonso, F. Goni, and L. Bagatolli, Biophys. J. **93**, 3548 (2007).
[8] T. Pott, H. Bouvrais, and P. Méléard, Chem. Phys. Lipids **154**, 115 (2008).
[9] J. I. Pavlic, J. Genova, G. Popkirov, V. Kralj-Iglic, and A. Iglic, Chem. Phys. Lipids **164**, 727 (2011).
[10] W. Helfrich, Z. Naturforsh. Teil C **28**, 693 (1973).
[11] R. Kwok and E. Evans, Biophys. J. **35**, 637 (1981).
[12] E. Evans and D. Needham, Faraday Discuss. Chem. Soc. **81**, 267 (1986).
[13] E. Evans and W. Rawicz, Phys. Rev. Lett. **64**, 2094 (1990).
[14] W. Harbich and W. Helfrich, Z. Naturforsh. Teil A **34**, 1063 (1979).
[15] M. Kummrow and W. Helfrich, Phys. Rev. A **44**, 8356 (1991).
[16] M. D. Mitov, P. Méléard, M. Winterhalter, M. I. Angelova, and P. Bothorel, Phys. Rev. E **48**, 628 (1993).
[17] S. Kakorin and E. Neumann, Ber. Bunsenges. Phys. Chem. **102**, 670 (1998).
[18] R. Graciá, N. Bezlyepkina, R. L. Knorr, R. Lipowsky, and R. Dimova, Soft Matter **6**, 1472 (2010).
[19] C. H. Lee, W. C. Lin, and J. Wang, Phys. Rev. E **64**, 020901 (2001).
[20] R. M. Servuss, W. Harbich, and W. Helfrich, Biochim. Biophys. Acta **436**, 900 (1976).
[21] M. B. Schneider, J. T. Jenkins, and W. W. Webb, Biophys. J. **45**, 891 (1984).
[22] H. Engelhardt, H. P. Duve, and E. Sackmann, J. Phys. Lett. (Paris) **46**, L395 (1985).
[23] H. P. Duwe, H. Engelhardt, A. Zilker, and E. Sackmann, Mol. Cryst. Liq. Cryst. **152**, 1 (1987).
[24] I. Bivas, P. Hanusse, P. Bothorel, J. Lalanne, and O. Aguerre-Chariol, J. Phys (Paris) **48**, 855 (1987).
[25] J.-F. Faucon, M. D. Mitov, P. Méléard, I. Bivas, and P. Bothorel, J. Phys. (Paris) **50**, 2389 (1989).
[26] M. D. Mitov, J.-F. Faucon, P. Méléard, and P. Bothorel, in *Advances in Supramolecular Chemistry*, edited by G. W. Gokel (JAI, New York, 1992), p. 93.
[27] P. Méléard, C. Gerbeaud, T. Pott, L. Fernandez-Puente, I. Bivas, M. D. Mitov, J. Dufourcq, and P. Bothorel, Biophys. J. **92**, 2616 (1997).
[28] P. Méléard, T. Pott, H. Bouvrais, and J. H. Ipsen, Eur. Phys. J. E **34**, 116 (2011).
[29] J. Genova, V. Vitkova, L. Aladgem, and M. D. Mitov, J. Optoelectron. Adv. Mater. **7**, 257 (2005).
[30] J. Pécréaux, H.-G. Döbereiner, J. Prost, J.-F. Joanny, and P. Bassereau, Eur. Phys. J. E **13**, 277 (2004).
[31] P. Usenik, T. Vrtovec, F. Pernus, and B. Likar, Med. Biol. Eng. Comput. **49**, 957 (2011).
[32] D. Marsh, Chem. Phys. Lipids **144**, 146 (2006).
[33] J. F. Nagle, Faraday Discuss. **161**, 11 (2013).
[34] V. Vitkova, K. Antonova, G. Popkirov, M. D. Mitov, Y. A. Ermakov, and I. Bivas, J. Phys.: Conf. Ser. **253**, 012059 (2010).
[35] J. Genova and J. Pavlic, Bulg. J. Phys. **39**, 65 (2012).
[36] S. T. Milner and S. A. Safran, Phys. Rev. A **36**, 4371 (1987).
[37] I. Bivas, Phys. Rev. E **81**, 061911 (2010).